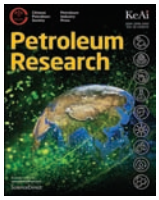
Petroleum Research 11 (2026) 101–115

Contents lists available at ScienceDirect

Petroleum Research

journal homepage: http://www.keaipublishing.com/en/journals/petroleum-research/



Full Length Article

Deep learning supported uncertainty quantification of core saturation measurements

Klemens Katterbauer *, Atul Godbole

Saudi Aramco, Saudi Arabia

ARTICLE INFO

Article history:
Received 28 October 2024
Received in revised form
11 June 2025
Accepted 20 June 2025
Available online 2 July 2025

Keywords:
Core analysis
Uncertainty quantification
Deep learning
Oil saturation estimation
Costa model

ABSTRACT

Core extraction and analysis are fundamental components of reservoir development. Core samples provide continuous vertical sections of the subsurface, enabling detailed visual assessment of depositional sequences and variations in reservoir characteristics. A thorough examination of these cores yields critical information significantly contributing to understanding and optimizing reservoir development. This data can include direct evidence of hydrocarbons' presence, quantity, spatial distribution, and production potential. The analysis of core samples is vital for understanding the pore system properties within potential reservoir intervals. Insights derived from core data improve the ability to predict reservoir performance and inform the selection of strategies to maximize cost-effective hydrocarbon recovery. This study employs a representative dataset from the Arabian Peninsula, specifically within the United Arab Emirates, using the Costa model as a supporting framework. The analysis incorporates the largest and smallest available sample sizes to ensure the final results remain within an acceptable range of variation. Each input parameter—core length, diameter, weight, fluid volumes, oil density, brine salinity (ppm), and brine density—is systematically varied to evaluate its impact on key reservoir properties, including saturation, porosity, permeability, and grain density. Additionally, the study investigates the effects of various combinations of incorrect input parameters to assess their influence on overall measurement accuracy. This methodology underpins a novel, AI-driven approach to uncertainty estimation in reservoir analysis. This approach enables more accurate assessment and informed decision-making in reserve estimation and reservoir management by quantifying the uncertainty in core-derived measurements.

© 2025 Chinese Petroleum Society. Publishing services by Elsevier B.V. on behalf of KeAi Communications Co. Ltd. This is an open access article under the CC BY-NC-ND license (http://creativecommons.org/licenses/by-nc-nd/4.0/).

1. Introduction

Core analysis is crucial in evaluating subsurface formations, particularly in the oil and gas industry. Geologists and engineers can understand the rock properties and depositional sequences that make up the reservoir by extracting a continuous, vertically oriented sample of the formation, known as a core. Core analysis directly measures the formation's rock properties, such as porosity, permeability, mineral composition, and residual saturations, which are essential for characterizing the reservoir's potential for hydrocarbon production. The vertical continuity of the core sample allows for the visual analysis of depositional sequences, including the identification of different facies, bedding planes, and other geological features that can impact reservoir quality and performance (Knackstedt et al., 2005; Yousef and Morozov, 2024). This information may prove hydrocarbons' existence, amount, distribution, and deliverability. Understanding the pore system's characteristics in the prospective reservoir unit requires units of cores. The knowledge gathered from cores improves the capacity to forecast reservoir performance and choose techniques to optimize economic hydrocarbon recovery (Rothwell and Rack, 2006; Yang et al., 2020).

Prior to the development of core acquisition techniques, information was gathered from drill cuttings from the well bore. The first continuous cores were acquired in the late 1800s (1887 by a Canadian geologist, Dr. Thomas W. Edwin, while working for the Standard Oil Company of Ohio). The core was approximately one inch in diameter and 10 feet long. Innovations and technological

* Corresponding author.
E-mail addresses: klemens.katterbauer@aramco.com (K. Katterbauer), atul.godbole@aramco.com (A. Godbole).

Peer review under the responsibility of Editorial Office of Petroleum Research.

https://doi.org/10.1016/j.ptlrs.2025.06.004
2096-2495/© 2025 Chinese Petroleum Society. Publishing services by Elsevier B.V. on behalf of KeAi Communications Co. Ltd. This is an open access article under the CC BY-NC-ND license (http://creativecommons.org/licenses/by-nc-nd/4.0/).

advancement have now facilitated core acquisition in virtually any environment, lithology, and length (Luffel and Guidry, 1992; Rothwell and Rack, 2006). The longest continuous core ever extracted is approximately 12,800 feet (3900 m) long, and it was extracted from the Sakhalin-1 oil field, located off the coast of Sakhalin Island, Russia. The core was extracted in 2011 by the ExxonMobil-led consortium, which operates the Sakhalin-1 project (Abbas et al., 2018). The core sample was extracted from a depth range of approximately 6500 to 19,300 feet (2000 to 5900 m). Core samples can be acquired during the exploratory, development, secondary, and tertiary recovery stages, thus enabling a better understanding of the subsurface (Morriss et al., 1997).

Typically, the process of extraction and exploitation of hydrocarbon reserves starts with prospecting (exploration), developing and primary extraction (production), and finally, secondary or tertiary extraction (enhanced oil recovery). During the exploratory phase, much of the subsurface is an unexplored entity. Hence, while drilling a well, inferences are made from the drilling cuttings. After reaching the target depth and logging the well, sidewall cores are acquired from prospective zones using wireline methods (Ameen et al., 2009). Extracting isolated samples, known as sidewall cores, from the wellbore face provides an alternative to continuous coring (Anis and Siddiqui, 2015). The lithology, petrology, porosity, permeability, and hydrocarbon concentration of the formation can all be inferred from these samples. The analytical results can validate log analysis computations (Luffel and Guidry, 1992). During the development phase of a well, the downhole environment is well understood, and continuous cores can be extracted in controlled conditions. The diameter of the core can range from 2½ inches to 7 inches, depending on the borehole size, specific requirements of the project, and the type of coring assembly being used. The length of the core can also vary, but it is not uncommon for continuous cores to be cut in lengths of up to 120 feet (Morriss et al., 1997).

1.1. Core analysis methods

In order to assess core samples, several sampling and analytical methods have been developed. These are detailed in API-RP-40. The kind of recovered core, its lithology, and the makeup of the pore system all influence the technique selection. There are three forms of core analysis: (1) whole core analysis, (2) conventional or plug analysis, and (3) sidewall core analysis. In order to identify net pay, hydrocarbon-water transition zones, contact levels, and formation boundaries, the core sampling frequency must be sufficient. The most representative sample inside each foot can be chosen, or sampling can be done statistically at the midpoint of each foot (Hirsaki et al., 1990). Typically, conventional core analysis plugs are collected three to four times each meter or once per foot to determine the variation in the physical and chemical properties of the rocks under consideration. This method works best in reasonably homogeneous pore systems, implying that the variations in the three basic parameters of lithology, porosity, and permeability are limited. Determining the properties of subsamples, typically 1″ in diameter by 2 inches long or 1.5 inches in diameter x 3 inches long, is the preferred method for core characterization. The continuous core is subsampled at regular (fixed) intervals. This method also simplifies statistical analyses of the rock properties. More frequent sampling is necessary due to variations in lithology or pore system development.

Heterogeneous formations show variations in rock properties and could also be defined by fractures, solution vugs, or irregularly developed pore systems. Sampling heterogeneous cores using the “sampling” method described in the paragraphs above is impractical and may result in misleading data. The properties of the plug samples are at that point only; the values represented by the plug sample may not represent the section from where the sample was acquired. Where practical, the entire core is used to determine the properties of the rocks. Core sample length limitation depends upon the equipment used to determine the properties. The whole core samples deal with larger volumes of the rock compared to plug samples. Hence, the average properties are more representative of the interval under consideration. Coping with larger volumes also increases the accuracy of measurements compared to plug samples (Arns et al., 2005).

1.2. Routine core analysis

The process of generation of Routine Core Analysis data is based on simple basic principles of physics. Measurement of weight, length, diameter, fluid volumes, gas flow rate, and application of Archimedes Principle, Boyles Law, and Darcy's Law (Ganat, 2024). API RP-40 does a commendable job of documenting the techniques available, procedures to be followed for each method, the calculations involved, the acceptable error margins, and even the reporting formats. This document has remained unchanged since 1998, and there has been little change in the principles of data generation (Forbes, 1998). Reservoir engineers and petrophysicists may encounter disagreements on the fact that the maximum physical damage to the core and, hence, its properties have been done during the core acquisition, core retrieval, surface core handling in the field, and transportation from the well site to the laboratory phase rather than during laboratory core processing, sample acquisition, sample cleaning, and measurements (Knackstedt et al., 2005).

Petrophysicists generally debate the accuracy of core analysis results given the challenge of matching the data generated from the core at a specific point scale to extrapolate it to the various scales going from the core to the reservoir scale. The industry-accepted reference is suggested by Thomas and Pugh, who, in their published technical paper - A Statistical Analysis of the Accuracy and Reproducibility of Standard Core Analysis (1989), discusses the variation in final results based on laboratory analyses. Technical documents that have subsequently followed this subject have resulted in a repetition of similar ideas and findings, with the main difference being the presentation style, language, and graphical representation (Pugh and Thomas, 1989). None have commented on the practical aspect of errors in raw data and the variation in the final results. Laboratories that give us routine core analysis data generally provide us with accurate data, provided all the processes involved in data generation follow the QA/QC protocols. When Core Analysis Results do not match the logs, it is always assumed that the log data is correct.

The magnitude of error in the final results depends on the sample size. Hence, this paper considers the most significant and most minor practically possible sample size for comparative purposes to calculate the final results. Each input parameter, like length, diameter, weight, volume, oil density, brine ppm, and brine density, is varied, and Saturation, Porosity, Permeability, and Grain Density Values are calculated (Adesida et al., 2011; Haghshenas et al., 2016). By understanding the accuracy and limitations of core analysis data, you can determine the maximum practical allowable error in input values that will still generate “industry-acceptable” results. A tolerance or margin of error for the input values can be defined to ensure the analysis results are still reliable and accurate enough to be useful for decision-making (Shafer, 2013).

Additionally, an attempt has been made to use various combinations of erred inputs to determine the effects on the final results

(Qajar and Arns, 2022). The paper uses representative data based on the Arabian Peninsula in the UAE supported by the Costa model, typically the most significant and smallest sample size. By varying each commonly measured input parameter, length, diameter, weight, volume, oil density, brine ppm, and brine density, you can determine the maximum allowable error for each parameter that will still allow the results to fit within an acceptable range of variation. This approach systematically evaluates the sensitivity of the results to each input parameter and determines the permissible range of variation for each parameter (Liu et al., 2021; Okoli et al., 2023). It also tries to use various combinations of erred inputs to determine the effects on the final results. Based on this, a new AI-driven framework for estimating uncertainty in core measurements and analyzing the impact of the various factors on the overall uncertainty.

2. Methodology

Two sidewall coring methods are used in the industry today: Percussion sidewall coring and rotary sidewall coring. Both these methods are used after the well bore has been drilled. A small piece of the formation at selected specific depths is acquired. These methods are typically used during the exploratory phase, where much of the bottom-hole conditions are unknown. Any sidewall coring procedure can recover cores for sidewall core analysis. Hard, well-cemented formations' percussion sidewall cores undergo significant alterations throughout the coring process and typically may not yield accurate assessments of their mechanical and petrophysical characteristics (Yousef and Morozov, 2024).

2.1. Core analysis methodology

Rotary sidewall coring is capable of acquiring 1.5-inch diameter x 2-inch long samples. A wireline activates the bit, extends into the formation, acquires a core sample, retracts, and deposits the sample in a sample chamber (Abbas et al., 2018). Rotary sidewall cores yield much better results as the process of rotary sidewall core acquisitions is similar to the conventional whole core acquisition. The Dean-Stark Method, as described in API RP-40, is a widely used technique for assessing the remaining oil and water volumes in core samples. The method involves using a specialized apparatus known as the Dean-Stark apparatus to extract and separate the oil and water from the core sample (Arns et al., 2005). The process begins by loading the core sample into the Dean-Stark apparatus (Fig. 1), which consists of a round-bottom flask, a condenser, and a graduated receiving tube. A pre-distilled organic solvent, which does not mix with water and has a boiling point greater than that of water, is added to the flask and heated to boiling point. The solvent vapors rise through the chamber and pass through the core sample, extracting the oil and water from the sample (Fig. 2). The vapors are then cooled in the condenser, causing the solvent, oil, and water to condense and fall into the graduated receiving tube. Since water is denser than the solvent, it separates and collects at the bottom of the tube, while the solvent and oil rise to the top. The water extracted from the sample can be read directly from the graduated tube (Patrick Murphy et al., 1996).

The core sample then undergoes further cleaning to remove any residual salts and heavier oil components. This may involve washing the sample with a solvent or using other cleaning methods. By taking the sample weights at various stages of the process, the volume of oil and formation brine in the sample can be calculated. Determining pore volume (PV) is described in detail below. The process begins by determining Grain Volumes (Gao et al., 2015).

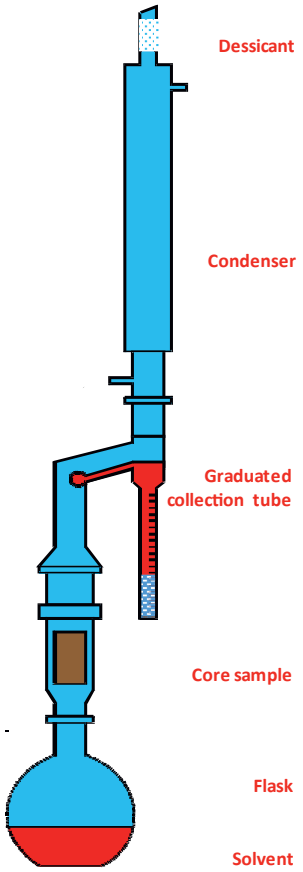


Fig. 1. Graphical illustration of the Dean-Stark process.

Grain volumes (GV) are measured using Boyle's law technique, which requires knowledge of the weight of the clean, dry sample, then the grain density can be as follows (Fig. 3). Grain Volume is measured using Boyle's Law, which states as follows.

$$P_1 \, x \, V_1 = P_2 \, x \, V_2 \tag{1}$$

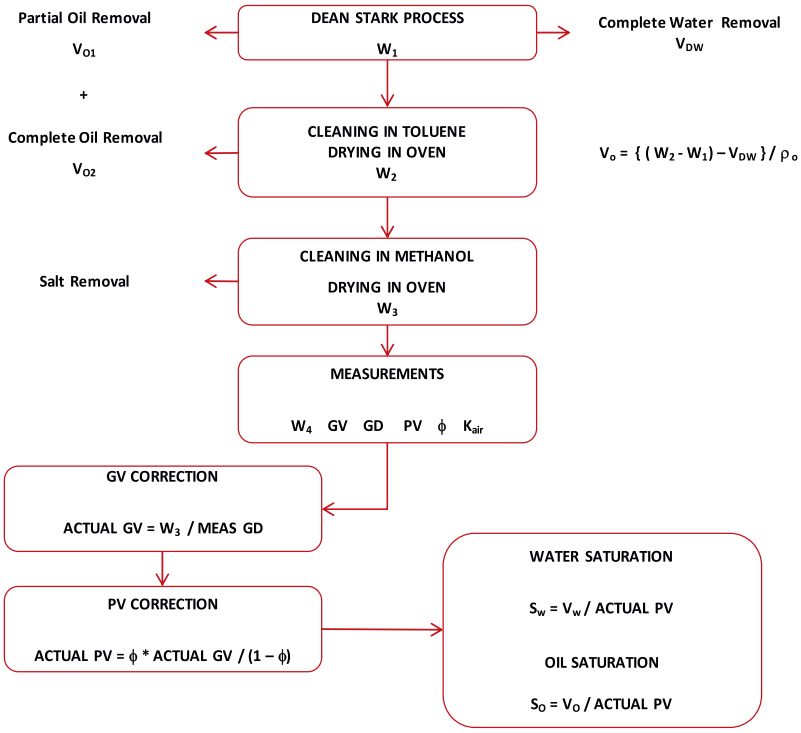
A reference cell of known volume (V_1) is pressurized with Helium gas. The stabilized pressure (P_1) is noted. This gas can expand into a chamber of known volume (V_2) containing the sample. The pressure drops, and the stabilized pressure (P_2) is noted (Gaafar et al., 2015; Qajar and Arns, 2022). Using Boyles Law, grain Volume V_g is calculated as follows:

$$P_1 \, V_1 = P_2 \, (V_1 + V_2 - V_g) \tag{2}$$

For accurate measurement of grain volumes, there are several requirements, such as the temperature having to be constant, the compressibility factor having to be equal to 1, and the valve displacement volume having to be zero. Furthermore, one assumes that the transducer has an accuracy of 0.05 % Full Scale and that the 4th-degree polynomial fit for the calibration is linear with an R^2 (fit) value of 1 (Hirsaki et al., 1990). If the sample is cylindrical, then bulk volume can be easily calculated, and hence, the pore volume and porosity are computed as follows:

$$\text{Porosity} = 100 * \frac{\text{Pore Volume}}{\text{Bulk Volume}} \tag{3}$$

If the samples are irregular in shape, then the clean samples are saturated with a fluid of known density, and the pore volumes are



W_1 = Weight of sample before Dean Stark
= Weight of Dry Sample + Weight of Water + Weight of Oil

V_{Br} = V_{DW} x Correction Factor

S_w = V_{Br} / PV

W_{DW} = Volume of Water Extracted

W_2 = Weight of Sample after Dean Stark
= Weight of Sample before Dean Stark - W_{DW} – W_o

$V_O = \{ (W_2 - W_1) - V_{DW} \} / \rho_o$

$S_o = V_o$ / PV

Fig. 2. Dean-Stark process diagram description.

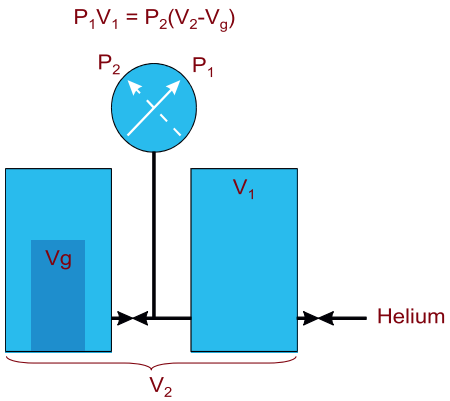


Fig. 3. Core measurement sample illustration.

estimated using the weight difference and the density of the saturating fluid (Yang et al., 2020). These samples can also be injected with mercury under high pressure to determine the pore volumes.

$$\text{Porosity} = 100 * \frac{\text{Pore Volume}}{\text{Bulk Volume} + \text{Pore Volume}} \tag{4}$$

The capillary pressure curves can also be determined if the mercury is injected in continuous pressure steps. We can determine the remaining oil (S_o) and water saturations (S_w) by knowing the extracted fluid and pore volumes, where PV is the pore volume, V_o the volume of oil, and V_w the water volume.

$$S_o = 100 * \frac{V_o}{PV} \tag{5}$$

$$S_w = 100 * \frac{V_w}{PV} \tag{6}$$

The analyses and the interpretation of results for vuggy samples require a sample-by-sample investigation and an estimation of the margin of error associated with the results. Reservoir rock is composed of water and gaseous and liquid hydrocarbons at depths. Depending on the reservoir type (oil, gas, or condensate) and the extent of charging, the specific fluids present and their relative quantity will vary. The distribution of fluids at or near the surface differs significantly from reservoir conditions. Drilling

procedures, gas expansion, and handling errors may necessitate these modifications. Generally, sidewall cores do not yield accurate saturation values compared to the results obtained from continuous cores. While acquiring conventional cores, the mud overbalanced pressure causes the mud filtrate to invade the core. Subsequently, a layer of mud cake around the periphery of the core prevents further mud filtrate invasion. In sidewall cores, the mud pressure acts on a very small surface area, and hence, the filtrate invasion is greater and much faster, and the formation of the mud cake is generally not observed (Gaafar et al., 2015). The degree to which sidewall and conventional continuous core residual oil saturations agree varies depending on the properties of the oil. Sidewall core oil saturation levels are marginally lower than traditional core analysis when oil gravity is between 35° and 40° API. Sidewall core oil saturations are 10–20% lower than conventional core saturations as oil gravity and viscosity rise. Sidewall cores in gas condensate zones have measured oil saturations that match or slightly exceed traditional core values.

2.2. Deep learning methodology

The gradient-boosting regressor framework was utilized to develop the AI-driven uncertainty quantification framework. Gradient boosting is a machine learning strategy based on boosting in a functional space, where the conventional residuals used in classic boosting are not the aim. Instead, these are the pseudo-residuals that are in the functional space (Chen et al., 2023). It provides a prediction model in the form of an ensemble of weak prediction models, or models that, usually consisting of straightforward decision trees, make very few assumptions about the data. Gradient-boosted trees are the name of the resulting algorithm when a decision tree serves as the weak learner, and it often performs better than a random forest (Sun et al., 2020). Similar to previous boosting techniques, a gradient-boosted tree model is constructed step-by-step. However, it differs from the other methods in that it permits the optimization of any differentiable loss function (Sun et al., 2020).

Like other boosting techniques, gradient boosting iteratively merges weak "learners" into a single strong learner. The least-squares regression setting makes it easiest to understand. In this setting, for the model F to predict values in the form $\widehat{y} = F(x)$, the objective is to minimize the mean squared error

$$\frac{1}{n}\sum_{i}(\widehat{y}_i - y_i)^2 \tag{7}$$

where i indexes over some training set of size n of actual values of the output variable y: $\widehat{y}_i$ is the predicted value $F(x_i)$, y_i is the predicted value $F(x_i)$.

The consideration for a gradient boosting algorithm with M stages, then at each of the m ($1 \le m \le M$) stages of the gradient boosting, an imperfect model F_m is developed. For small m, the model returns $\widehat{y}_i = \overline{y}$, implying that it is the mean of y. In order to improve the model, the new estimator $h_m(x)$ is added.

This implies that:

$$F_{m+1}(x_i) = F_m(x_i) + h_m(x_i) = y_i \tag{8}$$

or similarly:

$$h_m(x_i) = y_i - F_m(x_i) \tag{9}$$

This implies that the gradient boosting will fit h_m to the residual of $y_i - F_m(x_i)$, and F_{m+1} aims to minimize the errors of the predecessor function of F_m.

The observation that residuals $h_m(x_i)$ for a given model are proportional to the negative gradients of the mean squared error (MSE) loss function (with respect to $F(x_i)$) leads to a generalization of this idea to loss functions other than squared error as well as to classification and ranking problems:

$$L_{MSE} = \frac{1}{n}\sum_{i=1}^{n}(y_i - F(x_i))^2 \tag{10}$$

$$-\frac{\partial L_{MSE}}{\partial F(x_i)} = \frac{2}{n}(y_i - F(x_i)) = \frac{2}{n}h_m(x_i) \tag{11}$$

Therefore, generalizing gradient boosting would mean "plugging in" a different loss and its gradient. Gradient boosting might thus be specialized to a gradient descent algorithm. The gradient-boosting regressor framework is utilized to determine and estimate the saturation levels for both oil and water and the degrees of uncertainty that arise (Khan and Kirmani, 2024; Sun et al., 2020). In order to assess the impact of the various measurements on the saturation levels, a shapley feature importance analysis approach was utilized (Rao et al., 2019).

2.3. Feature importance methodology

In cooperative game theory, a solution idea is the Shapley value. It bears Lloyd Shapley's name, who introduced it in 1951 and was awarded the 2012 Nobel Memorial Prize in Economic Sciences. It allocates a distinct allocation (among the participants) of the total surplus produced by the cooperation of all players to each cooperative game. A group of appealing characteristics defines the Shapley value (Chen et al., 2023). A coalitional game is defined formally as: A function φ transfers subsets of players to the real numbers for a given set N (of n players):

$$\varphi : 2^N \to \mathbb{R} \tag{12}$$

where $\varnothing$ indicates the empty set, and $\varphi(\varnothing) = 0$. Furthermore, φ is referred to as a characteristic function. The function φ means that if S is a coalition of players, then the total expected amount of payoffs that the members of S can get through cooperation is described by $\varphi(S)$, also known as the worth of coalition S (Kumar et al., 2020).

Assuming all participants cooperate, one way to divide their overall rewards is using the Shapley value. As the only distribution with the desirable qualities mentioned below, it qualifies as "fair". In a coalitional game (φ, N), player i is assigned an amount that is determined by the Shapley value (Rao et al., 2019).

$$\begin{aligned} f_i(\varphi) &= \sum_{S \subseteq N \setminus \{i\}} \frac{|S|!(n - |S| - 1)!}{n!}(\varphi(S \cup \{i\}) - \varphi(S)) \\ &= \frac{1}{n}\sum_{S \subseteq N \setminus \{i\}} \binom{n-1}{|S|}^{-1}(\varphi(S \cup \{i\}) - \varphi(S)) \end{aligned} \tag{13}$$

where n is the total number of players, and the sum covers all subsets S of N, including the empty set that does not contain player i. Also, take note that the binomial coefficient is $\binom{n}{k}$. This formula can be understood as follows: for each actor, take the average of their contributions over all possible combinations in which the coalition can be formed. Imagine the coalition being formed one actor at a time, with each actor demanding their contribution $\varphi(S \cup \{i\}) - \varphi(S)$ as a fair compensation. Another comparable formula to calculate the Shapley value is:

$$f_i(\varphi)=\frac{1}{n!}\sum_{R}\left[\varphi\left(P_i^R\cup\{i\}\right)-\varphi\left(P_i^R\right)\right] \tag{14}$$

Here, P_i^R is the set of players in N that come before i in order R, and the total spans over all $n!$ orders R of the players.

Lastly, it can also be stated as:

$$f_i(\varphi)=\frac{1}{n}\sum_{S\subseteq N\setminus\{i\}}\binom{n-1}{|S|}^{-1}(\varphi(S\cup\{i\})-\varphi(S)) \tag{15}$$

It might be understood as:

$$f_i(\varphi)=\frac{1}{\text{number of players}}\sum_{\text{coalitions excluding}}\frac{\text{marginal contributions of } i \text{ to coalition}}{\text{number of coalitions excluding } i \text{ of this size}} \tag{16}$$

According to the characteristic function φ it is possible to calculate the synergy that every player group offers. The special function is synergy. The expression $w:2^N\to\mathbb{R}$, so that the expression for any subgroup number of players, $S\subseteq N$. Put differently, the coalition's "total value". The value of S is obtained by adding the synergy of all potential subsets of S.

$$\varphi(S)=\sum_{R\subseteq S}w(R) \tag{17}$$

Considering a characteristic function φ, the function of synergy w is calculated as utilizing the principle of Inclusion Exclusion. Put another way, the coalition's synergy, the value that its subsets do not already account for, is S. The synergy function is used to express the Shapley values as follows:

$$w(S)=\sum_{R\subseteq S}(-1)^{|S|-|R|}\varphi(R) \tag{18}$$

$$f_i(\varphi)=\sum_{i\epsilon S\subseteq N}\frac{w(S)}{|S|} \tag{19}$$

where the sum is over all subsets S of N that include player i. This may be understood to mean:

$$f_i(\varphi)=\sum_{\text{coalitions including } i}\frac{\text{synergy of the coalition}}{\text{members in the coalition}} \tag{20}$$

As stated differently, each coalition's synergy is distributed evenly among its members. A logical method for explaining the predictions of nonlinear models, which are frequently used in machine learning, is the Shapley value. Shapley values give a natural way to determine which features contribute to a prediction or to its uncertainty by reading a model trained on a set of features as a value function on a coalition of players. This unites DeepLIFT, Layer-Wise Relevance Propagation, and locally Interpretable Model-Agnostic Explanations (LIME), among other methods (Kumar et al., 2020).

3. Results and discussion

The study outlines the novel uncertainty quantification framework for core analysis measurements, demonstrated on various core analysis measurements. The smaller the sample size, the greater the error. Hence, for all practical purposes, the smallest workable size for a sample to measure grain density, porosity, permeability, and fluid saturation is 1.5 inches in diameter and 1.5 inches in length. The smallest sample size and a range of porosities for the same sample density are considered. The study also assumes that the samples are homogenous, nonvuggy, and right cylinders. Archie's basic set of equations establishes the quantitative correlations between porosity, formation resistivity Rt, formation-water resistivity, and water saturation of reservoir rocks (Ganat et al., 2024a). Porosity and formation resistivity are derived from log data; however, porosity logs must be confirmed by core measurements taken at representative stress levels. The formation-resistivity-factor (F) and resistivity-index (I) tests on cores yielded the m and n values. Many petrophysicists have to rely on historical SCAL data that was often obtained under ambient conditions.

3.1. Core analysis uncertainty measurements

Porosity is frequently measured at stress in the formation-factor test along with core resistivity Ro, and the results are used to derive porosity-compaction factors for log calibration. According to a standard test methodology, the sample is unconfined and soaked in brine before being put into the test core holder following resistivity stabilization. In order to fill the system with brine before loading, air that is compressible and resistive must be eliminated from the annulus between the plug and the sleeve, the end stems, and the measurement system. In order to determine the correct pore-volume decrease under stress, the sleeve-conformance pressure (SCP) and sleeve-conformance volume (SCV) of brine in the plug/sleeve annulus must be satisfactorily established for each test plug. Small steps are taken to enhance the confining pressure while recording the core resistivity and pore-volume ejection. An inflection of the resistance or expelled-volume vs. confining-pressure curves typically identifies the SCP and SCV. Rarely are volume/stress statistics supplied, and regardless of the plug form and surface topology, many laboratories assume the same SCP (and consequently SCV) for every sample. The interpretation of SCP and SCV can be arbitrary, even when data are available. This has a noticeable impact on porosity measurements.

The extra salinity may significantly impact Archie's m and n value determination, creating additional measurement challenges. Brine adheres to the plug's surface during saturation in ambient-condition F measurements, but this is not a problem for tests conducted under stressful circumstances (over SCP). If this surface brine is left in place, it will act as a conduit for current flow and cause the measured resistivity to drop too low. A surface brine coating as thin as 2.5 μm in a low-porosity sample can lead to an approximate 30% underestimate of F. The ambient-condition resistivity index (Rt/Ro) and n will be excessively high if F (and Ro) are too low. Petrophysicists frequently are unable to work with data that eliminate these effects, even though both the F and I test must be measured under stress. Surface brine yields an average positive error of 15% in n and a negative error of 30% in m at ambient circumstances (Ganat et al., 2024b).

Calculating saturations from gravimetric data can be unreliable due to grain loss from manipulating plugs during testing. It is possible to interpret a weight loss during a drainage experiment as a loss of water, leading to a calculated water saturation value significantly lower than the actual value. A mere 2% dry weight grain loss for a 16%-porosity 140-g plug corresponds to a 20-saturation-unit mistake in water saturation for a gas/water test. The grain-loss error is larger since the fluid-density differential is lower in an oil/water system. Grain-loss correction aims to estimate the fluid-filled pore volume at every stage of handling and testing processes and, when practical, validate these approximations using measured data. Regretfully, these adjustments may be arbitrary. Historically, the primary source of core-derived saturation/height functions was mercury-injection capillary pressure data. Before the mid-1990s, most mercury-injection capillary pressure tests were conducted using manual equipment on core-plug samples with a diameter of one or 1.5 inches and a length of two to three inches, at injection pressures as high as 2000 psi. The core-plug helium pore and injected mercury volumes were used to calculate the nonwetting- and wetting-phase saturations.

These days, almost all measurements are performed using automated high-pressure machinery with injection pressures up to 55,000 psi. These devices were not intended for use with capillary pressure curves on core plugs; instead, they were made expressly for pore-size-distribution testing on papers, catalysts, porous materials, and ceramics. The bulk volume of standard core injection samples is about 5 mL, while the sample chambers (penetrometers) are limited to about 10 mL. As a result, the chip-sample pore volume for a 20% porosity sample is less than 1 mL, while the pore volume for a 1½ inch diameter × 2½ inch length plug is 14 mL. Since most laboratories inject mercury to define the total mercury-filled pore volume, volume errors significantly impact saturation estimated from immersion bulk volume and helium grain volume on tiny samples.

The capillary pressure versus water-saturation curves appear to be distorted in some formations due to high-pressure mercury injection. In the scenario covered in the full paper, tests on the chip samples were conducted on 4- to 6-mL specimens. In contrast, tests on the mercury-injection samples were performed on 1.5-in. plugs using traditional manual equipment. The test plugs were not contained in either instance (3D injection). The underlying distortion phenomena are still poorly understood. They seem more pronounced on materials with clay-filled micropores, which are typically inaccessible to mercury at 2000 psi. These might be associated with sample-size percolation dependencies. The pore system looks to be permanently and gradually damaged by continuous higher-pressure injection, significantly impacting how the end user creates saturation/height curves from high-pressure mercury injection data. The high-pressure-mercury-injection data on plug chips represent a distinct population, and when used blindly in isolation, they lead to hydrocarbon saturations that are overly optimistic. The arising uncertainty for these saturation measurements from cores may represent an important factor in evaluating and determining which parameters may significantly impact uncertainty quantification. The above-outlined methodology is evaluated using benchmark core sample data. We assume a sample with the data outlined in Table 1.

Grain density is calculated as the divisor between the grain weight and the grain volume, with the other parameters depending on the measurements of the sample weight, grain volume, sample length and diameter. In order to outline the impact, various scenarios are outlined. The first focuses on the error in the measurement of weight and its effect on grain density as outlined in Table 2.

Assuming that the measurement of grain volume is correct and there is an error in the measurement of weight. To keep the value of grain density within the acceptable limits of accuracy of ± 0.02 gms/cc, the maximum practical acceptable error in weight is 0.370 gms (Fig. 4). A sample having a porosity of 45 % can have a maximum error in weight of 0.370 gms whereas a sample of porosity 5 % can have a maximum error in weight of up to 0.620 gms to keep the grain density in the allowable range of ± 0.02 gms/cc. A sample with a higher porosity for the same bulk volume should have a lower acceptable error in weight than a sample with lower porosity.

The second scenario revolves around the error in the measurement of grain volume and its effect on Grain Density and porosity, as shown in Table 3.

Assume that the weight measurement is correct and there is an error in the measurement of grain volume. To keep the value of grain density within the acceptable limits of accuracy of ± 0.02 gms/cc, the maximum practical acceptable error in the measurement of grain volume is 0.240 cc. This will also allow the porosity to be kept within the acceptable error limits of 0.5 % PU. A sample of porosity

Table 1
Benchmark core sample basic data.

Sample number	Dry weight gms	Diameter cm	Length (1.5 inch) cm	Grain volume cc	Area cm2	Bulk volume = L x A cm3	Pore volume = BV - GV cc	Grain density = Weight/GV gms/cc	ϕ = 100 x (PV/BV) %
1	109.397	3.810	3.810	41.282	11.406	43.455	2.173	2.65	5.0
2	97.883	3.810	3.810	36.937	11.406	43.455	6.518	2.65	15.0
3	86.366	3.810	3.810	32.591	11.406	43.455	10.864	2.65	25.0
4	74.852	3.810	3.810	28.246	11.406	43.455	15.209	2.65	35.0
5	63.335	3.810	3.810	23.900	11.406	43.455	19.555	2.65	45.0

Table 2
First scenario with errors in the measurements.

Error in measurement of weight			
Sample number	Grain density = Weight/GV (gms/cc)	Phi = 100 x (PV/BV)	Maximum allowable error in weight (gms)
1	2.65	5	0.620
2	2.65	15	0.560
3	2.65	25	0.500
4	2.65	35	0.430
5	2.65	45	0.370

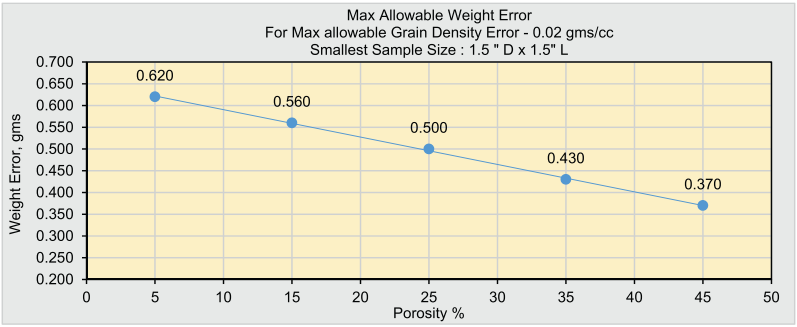


Fig. 4. Max allowable weight error for grain density.

Table 3
Error in measurement of the grain volume.

Error in measurement of grain volume (Small)				
Sample number	Grain density = Weight/GV (gms/cc)	Phi = 100 x (PV/BV)	Maximum allowable error in weight (gms)	Error in porosity (% PV)
1	2.65	5	0.230	0.53
2	2.65	15	0.210	0.48
3	2.65	25	0.190	0.44
4	2.65	35	0.160	0.37
5	2.65	45	0.140	0.32

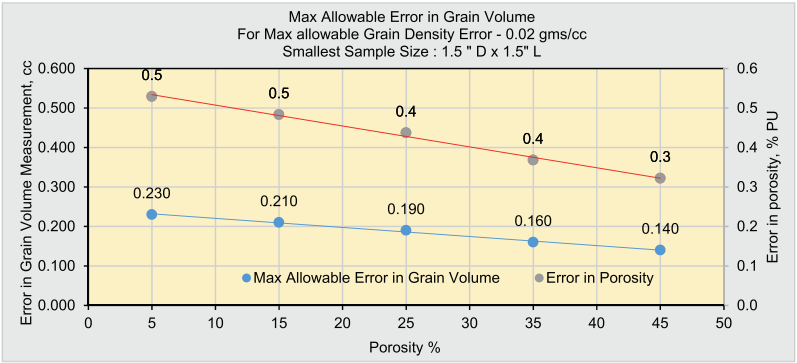


Fig. 5. Maximum allowable error in grain volume.

Table 4
Error in length and diameter.

Error in measurement of grain volume (Small)				
Sample number	Grain density = Weight/GV (gms/cc)	Phi = 100 x (PV/BV)	Maximum allowable error in length (mm)	Maximum allowable error in diameter (mm)
1	2.65	5	0.200	0.1
2	2.65	15	0.225	0.1
3	2.65	25	0.255	0.1
4	2.65	35	0.295	0.2
5	2.65	45	0.350	0.2

45 % can have an error of measurement of Grain volume of 0.140 cc to keep the grain density within acceptable range of ± 0.02 gms/cc and will lead to an error in porosity of 0.3 % PU (Fig. 5).

The third scenario revolves around the error in measuring length and diameter and its effect on porosity as outlined in Table 4.

Assume that all the measurements are correct and there is an error in the measurement of length. To keep the value of porosity within the acceptable limits of accuracy of ± 0.5 PU, the maximum practical acceptable error in length measurement is 0.2 mm. Assume that the diameter is in error. To keep the value of porosity within the acceptable limits of accuracy of ± 0.5 PU, the maximum practical acceptable error in measurement of diameter is 0.1 mm. A sample of porosity 45 % can have a maximum error of 0.17 mm in length or 0.35 mm in diameter to keep the porosity within 0.5 % PU (Fig. 6).

The next question for developing the framework is the saturation measurement, which is based on the dean stark method (Fig. 7). The extraction and measurement of fluid volumes and thus calculating saturation by the Dean stark process is today's most common method used in the oil industry. This requires the sample to go through a process requiring the measurement of weights and volumes and using the correct constants in the calculations. The sample is weighed and loaded into a Dean-Stark Apparatus, where the water is extracted using a solvent, collected, and measured. The solvent also partially extracts oil, thus leaving some oil and the salt (from the formation brine) in the sample. The sample is then cleaned using a soxhlet extraction method and a solvent to extract the oil completely. The sample is dried and weighed. The sample is then transferred into another soxhlet, which uses a different solvent to extract the salts. Once cleaned, the sample is dried and weighed again. Grain volume is measured, and Grain density, Pore Volume, and porosity are calculated using earlier methods. The primary sources of error are the Measurement of Weights during the weight measurement process, the measurement of extracted water volumes, Grain loss during the handling process, insufficient sample cleaning leading to residual oil or salts in the sample, and finally, the Incorrect oil density (or API gravity), brine salinity, density, and ppm.

In the next step, we investigate the error that arises from the oil density variation between 0.725 and 0.825 gm/cc as outlined in Table 5.

The maximum allowable weight of oil to allow for a maximum allowable error of ± 2.5 % PV error in oil saturation, the range of oil density from 0.725 to 0.825 gm/cc is 0.320 gm for a sample of 5.0 % porosity to 2.90 gms for a sample of 45% Porosity. This equates to an oil saturation of 20.4% (Fig. 8). Anything above these numbers will give you data beyond the acceptable range of error of ± 2.5 % PV for the density range under consideration.

Next we investigate the recovery that may arise from water salinity variations between 10000 and 100000 ppm. The maximum allowable volume of water recovered to allow for a maximum allowable error of ± 2.5 % PV error in water saturation in the range of brine salinity from 10000 to 100000 ppm is 1.85 cc for a sample of 5.0 % porosity to

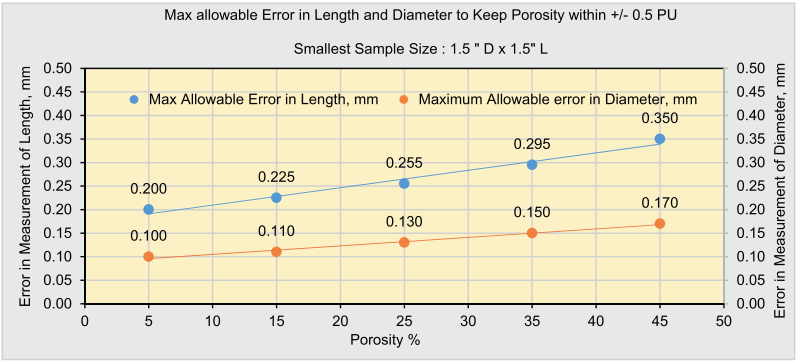


Fig. 6. Maximum allowable error in length and diameter.

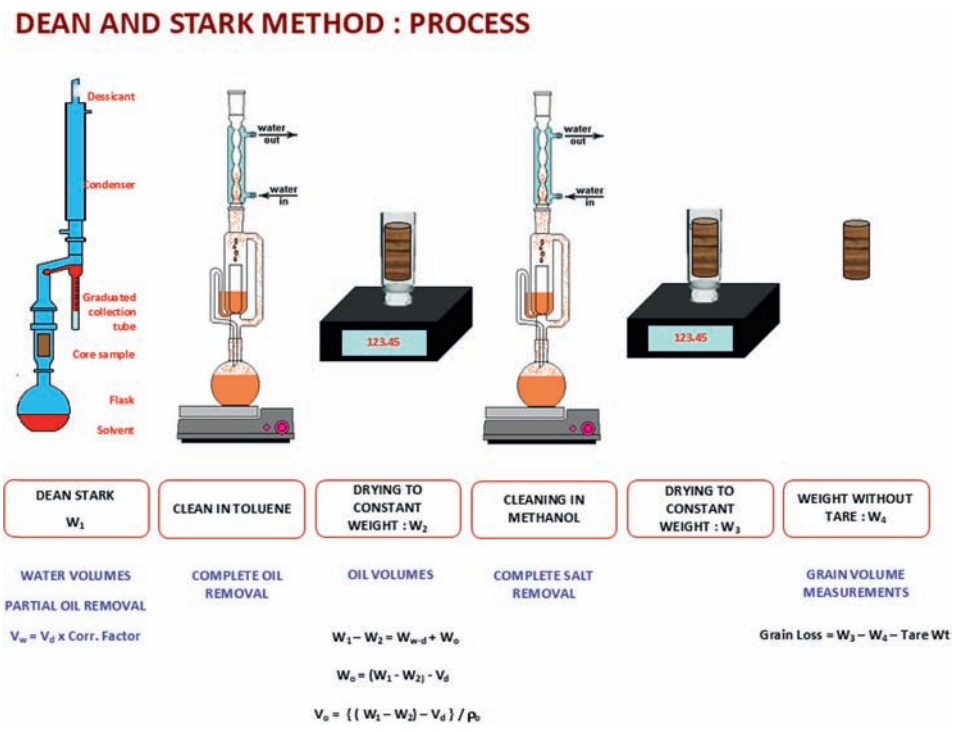


Fig. 7. Outline of the dean stark saturation measurement steps.

Table 5
Oil density variations.

Oil density 0.725–0.825 gm/cc		
Water Sal = 10,000–100,000 ppm		
Porosity	Wo (gms)	Vdw (cc)
5	0.320	1.85
15	0.960	5.50
25	1.600	9.10
35	2.250	12.80
45	2.900	16.40

Table 6
Oil and water density challenges.

Porosity, %	Oil density, gm/cc			Oil density, gm/cc		
	0.725	0.825	0.925	0.725	0.825	0.925
	Maximum allowable weight, gms			Maximum Allowable Oil Saturation, % PV		
5	0.370	0.424	0.476	23.5	23.7	23.7
15	3.550	4.087	4.583	75.1	76.0	76.0
25	7.533	8.572	9.611	95.6	95.6	95.6
35	10.604	12.067	13.529	96.2	96.2	96.2
45	13.676	15.563	17.449	96.5	96.5	96.5

16.4 cc for a sample of 45% porosity. Based on the analysis, the water saturation of the core sample is approximately 84.6% (Fig. 9). Anything above these numbers will give you data going beyond the acceptable error range of 2.5 % PV for the salinity range under consideration.

Finally, the following analysis focuses on the errors arising from grain loss, including errors in the oil saturation and lack of water in the sample. Assume all the weights taken have been correct until the sample is removed from the tare. There is a loss of grains between the last weight measurement of grain volume and the calculation of grain density. This will lead to a lower grain volume. Since the bulk volume is constant, the actual pore volume is lower than that calculated. Hence, the porosity is lower than the actual. The maximum allowable error for a sample for porosity remains within the specified error limits of ± 0.5 % PU (Table 6). The maximum permissible oil weight (for calculation of oil volume) to account for the porosity variation of ± 0.5 % PU depends upon the density of the oil in the sample. The oil saturation cannot exceed 100%; hence, we can limit the volume calculation to 96.5 % PV.

The maximum effect of the reduction in pore volumes is seen in samples with a porosity of up to 15 % PU. The oil saturation of any sample with a porosity of more than 15 % should not be affected by grain loss of up to 0.5 gms. For example, for a sample of Porosity 5 % PU, the maximum allowable weight of oil recovered is 3.550 gms, approximately 75.1 % PV. Any higher weights recorded will show erroneous saturation values (Fig. 10).

The subsequent analysis is based on the grain loss due to measurement errors in the water saturation and no oil in the sample. The maximum allowable error in grain loss for a sample for porosity to remain within the specified error limits of ± 0.5 % PU is 0.37 gms, as outlined in Table 7. This grain loss is allowable only if the sample has been kept in the tare all the time and the weights correctly measured. The maximum allowable distilled water extracted during the Dean-Stark process to account for the reduction in pore volume depends upon the density of the brine in the sample. The maximum effect of the reduction in pore volumes

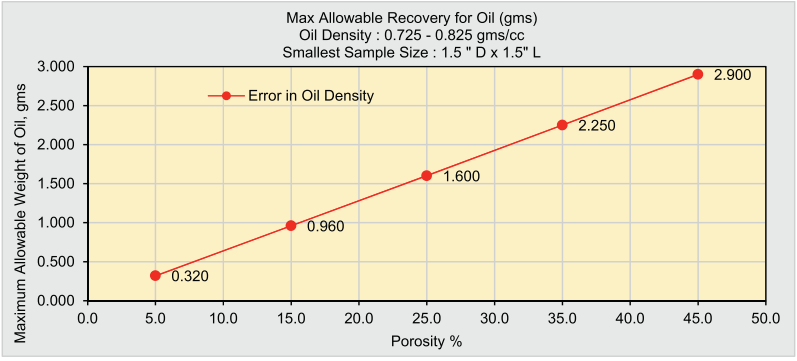


Fig. 8. Maximum allowable recovery for oil.

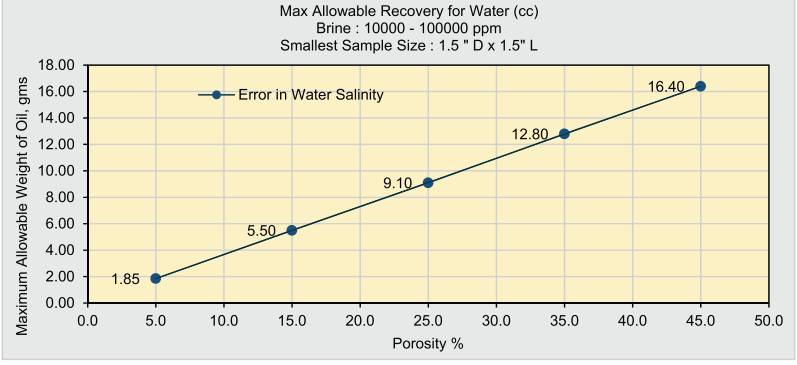


Fig. 9. Water salinity variations.

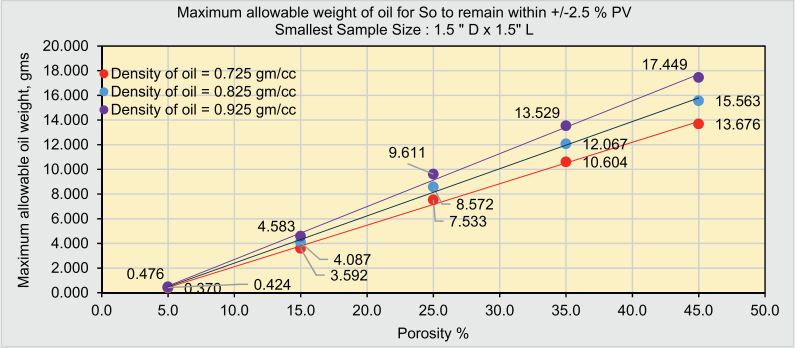


Fig. 10. Maximum allowable weight for oil.

Table 7
Water PPM.

Porosity, %	Water Ppm									
	10000	50000	100000	150000	200000	10000	50000	100000	150000	200000
	Maximum allowable extracted distilled water, cc					Maximum allowable water saturation, % PV				
5	0.51	0.51	0.50	0.49	0.48	23.6	23.8	23.8	23.8	23.8
15	4.94	4.88	4.80	4.70	4.59	76.0	76.0	76.1	76.0	76.0
25	10.35	10.23	10.06	9.86	9.64	95.6	95.6	95.6	95.6	95.7
35	14.58	14.41	14.16	13.89	13.57	96.2	96.2	96.2	96.2	96.3
45	18.80	18.58	18.26	17.92	17.50	96.5	96.5	96.4	96.6	96.5

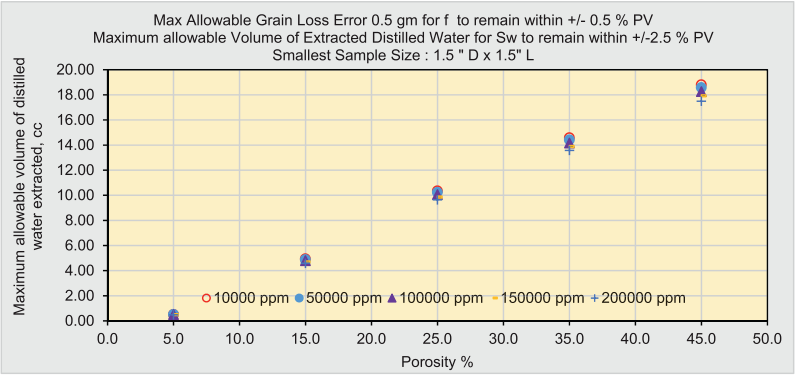


Fig. 11. Maximum allowable grain loss error.



Fig. 12. Drip erosion example.

is seen in samples with porosity of up to 15 % PU (Fig. 11). The water saturation of any sample with a porosity of more than 15 % should not be affected by grain loss of up to 0.5 gms.

The next is grain loss due to measurement errors in the water saturation, assuming there is no water in the sample. However, if the grains are lost during the dean stark extraction process (due to incorrect handling or drip erosion) and not accounted for, then this grain loss will be accounted for weight lost due to oil (Fig. 12). This will add to the calculated oil volumes. This grain loss can affect the calculation of grain volumes, hence the pore volumes and finally the porosity. Thus the samples may show an unreasonably high oil volume saturation. The total oil and water saturation may even exceed 100%. Grain loss affects pore volume measurements and porosity. Hence, the maximum allowable grain loss during drip erosion is to keep the saturation within the specified 2.5 % PU and keep the porosity within 0.5 % error band. Consider oil of density 0.725 gms/cc, then a sample having a porosity of 35 % and a S_o of 5 % is allowed a maximum of $\pm$ 0.277 gms of error in grain loss. Similarly, a sample having a

porosity of 35 % and a S_o of 90 % is allowed a maximum of ± 0.356 gms of error in grain loss (Fig. 13).

3.2. Uncertainty analysis

With this analysis undertaken, the framework's objective is to integrate the potential uncertainties to enhance oil and water saturation measurements. The arising uncertainty in the oil and water saturation estimates is exhibited in Figs. 14 and 15. Oil saturation estimates exhibit a long-tail distribution to the lower end of the figures with a mean of around 10 % of oil saturation. In contrast, the water saturation estimates exhibit a stronger Gaussian distribution with a narrow interval of water saturation estimates.

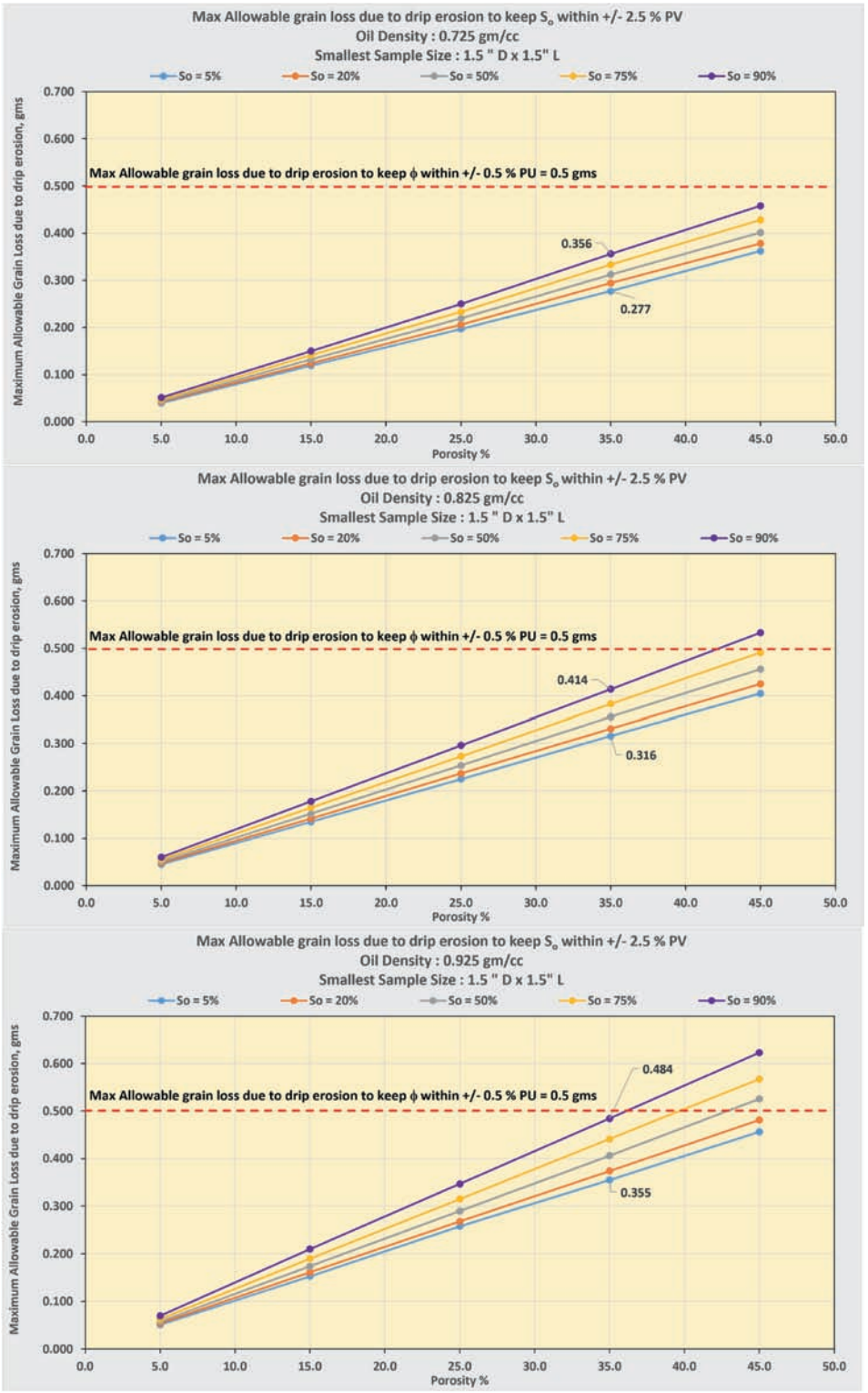


Fig. 13. Drip erosion induced errors.

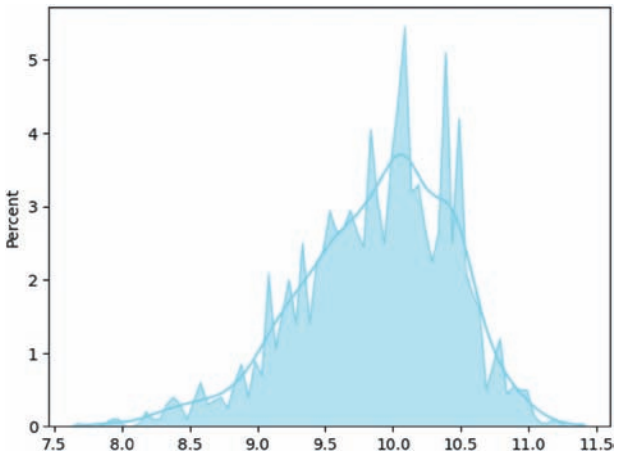


Fig. 14. Uncertainty estimates of the oil saturation.

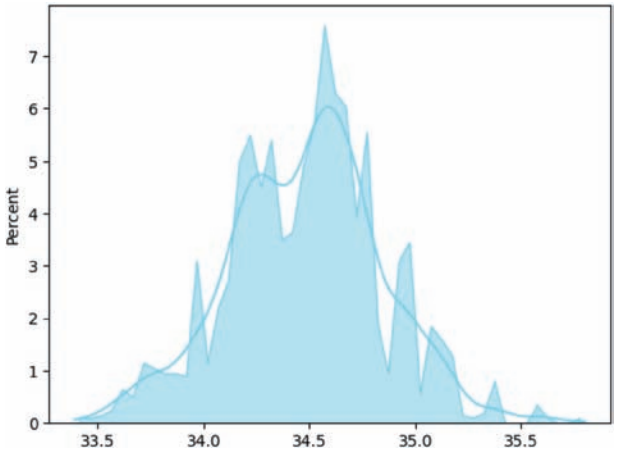


Fig. 15. Uncertainty estimation for the water saturation.

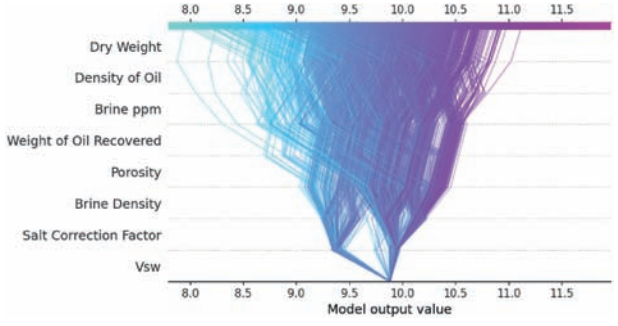


Fig. 16. Decision plot for Shapley values for S_o, the base value is 9.88 %.

A Shapley value analysis was conducted as outlined in Fig. 16 to evaluate the impact of the various parameters. The plot exhibits a decision plot that starts at the base value of 9.88 % to cover the entire range. The most significant factors are the amount of shale and the porosity that may significantly affect overall saturation estimates. Additionally, the brine density and ppm value significantly affect the estimates and the overall spread. For a single estimate, the impact of the various parameters on the oil saturation is outlined in Fig. 17, which exhibits that both brine density

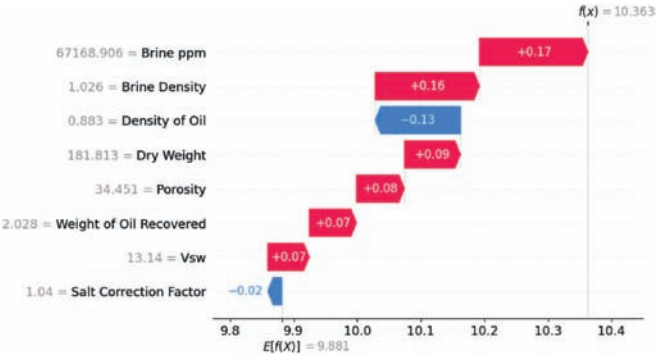


Fig. 17. Waterfall impact plot on the estimation of the oil saturation.

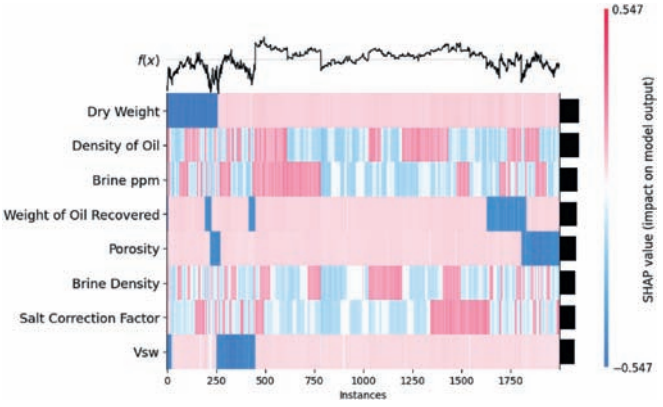


Fig. 18. Heatmap visualization of 2000 realizations outlining the critical features for S_o.

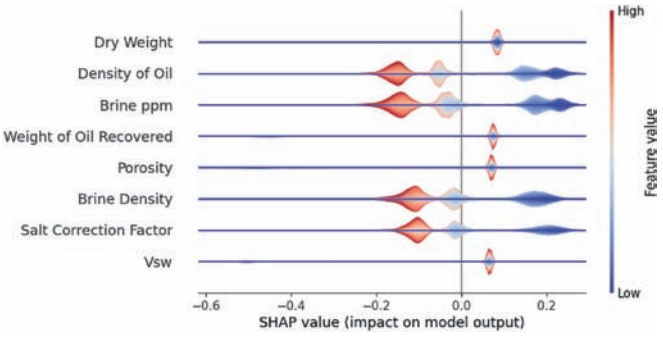


Fig. 19. Violin plot for SHAP values for S_o.

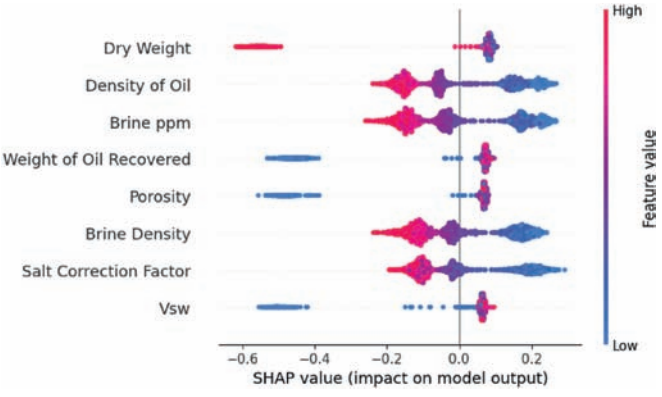


Fig. 20. SHAP value summary for oil saturation estimation (S_o).

and ppm significantly affect the final estimate. This can be confirmed by the relative impact over more than 2500 estimates, as shown in Fig. 18, which exhibits that both brine density and ppm have the most significant and uniform impact, while dry weight and the shale factor have a relatively limited impact with a few outlier values that lead to high reductions in the Shapley value.

The analysis is extended by Figs. 19 and 20, which indicate within a Violin plot the shape values for the estimation of the oil saturation, as well as the most significant factors arising from both the density of oil and brine and the brine-related salt concentrations. This, in particular, reduces overall oil saturation estimates and may impact the values. The results are supported by Fig. 20, which provides an overall SHAP value summary for the oil saturation estimation and arising uncertainty, indicating that uncertainty in the salt-related factors may significantly affect the uncertainty in the oil saturation estimates.

4. Conclusion

Core extraction and analysis play an essential part in reservoir development. Cores are a source of full, vertically continuous samples visually examining depositional sequences and reservoir character variations. Proper examination of cores yields information that may significantly support reservoir development. Direct evidence of the presence, quantity, distribution, and deliverability of hydrocarbons may be included in this data. Utilizing cores is essential to comprehend the properties of the pore system in the potential reservoir section. Knowledge from cores enhances our ability to predict reservoir performance and select methods to maximize cost-effective hydrocarbon recovery. In order to allow the final results to fit within the acceptable range of variation, the paper uses a set of representative data based on the Arabian Peninsula in the United Arab Emirates, supported by the Costa model. Typically, the largest and smallest sample sizes are used. Each input parameter is varied to determine the maximum allowable error for length, diameter, weight, volumes, oil density, brine ppm, and brine density on saturation, porosity, permeability, and grain density values. In order to ascertain the impact on the outcome, it additionally attempts to employ different combinations of incorrect inputs. This is the foundation for a novel AI-driven approach for estimating uncertainty in key measurements and examining how various factors affect the total amount of uncertainty. The uncertainty estimation enables us to efficiently assess and evaluate further analysis of the cores for accurate reserves estimation and management.

CRediT authorship contribution statement

Klemens Katterbauer: Writing – original draft, Software, Methodology, Formal analysis, Data curation, Conceptualization. **Atul Godbole:** Writing – review & editing, Validation, Supervision, Resources, Investigation, Formal analysis, Data curation.

Declaration of competing interest

The authors declare that they have no known competing financial interests or personal relationships that could have appeared to influence the work reported in this paper.

References

Abbas, A.K., Flori, R.E., Alsaba, M., 2018. Estimating rock mechanical properties of the Zubair shale formation using a sonic wireline log and core analysis. J. Nat. Gas Sci. Eng. 53, 359–369. https://doi.org/10.1016/j.jngse.2018.03.018.

Adesida, A., Akkutlu, Y., Resasco, D., Rai, C., 2011. Kerogen pore size distribution of barnett shale using DFT analysis and Monte Carlo simulations. In: SPE Annual Technical Conference and Exhibition. Denver, Colorado. https://onepetro.org/SPEATCE/proceedings/11ATCE/11ATCE/SPE-147397-MS/148794.

Ameen, M.S., Smart, B.G.D., Somerville, J. Mc, Hammilton, S., Naji, N.A., 2009. Predicting rock mechanical properties of carbonates from wireline logs (A case study: Arab-D reservoir, Ghawar field, Saudi Arabia). Mar. Petrol. Geol. 26 (4), 430–444. https://doi.org/10.1016/j.marpetgeo.2009.01.017.

Anis, M.D., Siddiqui, T.Z., 2015. Issues impacting sustainability in the oil and gas industry. J. Manag. Sustain. 5, 115.

Arns, C.H., Bauget, F., Sakellariou, A., Senden, T.J., Sheppard, A.P., Sok, R.M., Ghous, A., Pinczewski, W.V., Knackstedt, M.A., Kelly, J.C., 2005. Digital core laboratory: petrophysical analysis from 3D imaging of reservoir core fragments. Petrophys. - SPWLA J. 46 (4).

Chen, H., Covert, I.C., Lundberg, S.M., Lee, S.-I., 2023. Algorithms to estimate Shapley value feature attributions. Nat. Mach. Intell. 5 (6), 590–601. https://doi.org/10.1038/s42256-023-00657-x.

Forbes, P., 1998. The status of core analysis. J. Petrol. Sci. Eng. 19 (1), 1–6. https://doi.org/10.1016/S0920-4105(97)00030-2.

Gaafar, G.R., Tewari, R.D., Zain, Z.M., 2015. Overview of advancement in core analysis and its importance in reservoir characterisation for maximising recovery. In: SPE Asia Pacific Enhanced Oil Recovery Conference. Kuala Lumpur. https://doi.org/10.2118/174583-MS.

Ganat, T., 2024. Experimental investigation of viscous oil–water–sand flow in horizontal pipes. Petroleum 10 (2), 275–293. https://doi.org/10.1016/j.petlm.2023.09.005.

Ganat, T., Hrairi, M., Badawy, A., Khosravi, V., Abdalla, M., 2024a. Advancing sandstone reservoir compressibility prediction: a correlation-driven methodology. Petrol. Res. 9 (2), 273–279. https://doi.org/10.1016/j.ptlrs.2024.01.006.

Ganat, T., Hrairi, M., Badawy, A., Khosravi, V., Abdalla, M., 2024b. Advancing sandstone reservoir compressibility prediction: a correlation-driven methodology. Petrol. Res. 9 (2), 273–279. https://doi.org/10.1016/j.ptlrs.2024.01.006.

Gao, B., Kralik, J., Vo, L., Shebl, H., Al Shehhi, R., Al Jawhari, M.O., Fullmer, S., 2015. State of the art special core analysis program design and results for a middle eastern carbonate reservoir. In: Abu Dhabi International Petroleum Exhibition and Conference. https://doi.org/10.2118/177510-MS. Abu Dhabi.

Haghshenas, B., Clarkson, C.R., Aquino, S.D., Chen, S., 2016. Characterization of multi-fractured horizontal shale wells using drill cuttings: 2. Permeability/diffusivity estimation. J. Nat. Gas Sci. Eng. 32, 586–596. https://doi.org/10.1016/j.jngse.2016.03.055.

Hirsaki, G., Rohan, J., Dubey, S., Niko, H., 1990. Wettability evaluation during restored-state core analysis. In: SPE Annual Technical Conference and Exhibition. New Orleans. In: https://onepetro.org/SPEATCE/proceedings/90SPE/90SPE/SPE-20506-MS/67791.

Khan, S.Q., Kirmani, F.U.D., 2024. Applicability of deep neural networks for lithofacies classification from conventional well logs: an integrated approach. Petrol. Res. 9 (3), 393–408. https://doi.org/10.1016/j.ptlrs.2024.01.011.

Knackstedt, M., Kelly, J., Saadatfar, M., Senden, T., Sok, R., 2005. Rock fabric and texture from digital core analysis. In: SPWLA 46th Annual Logging Symposium. New Orleans.

Kumar, I.E., Venkatasubramanian, S., Scheidegger, C., Friedler, S.A., 2020. Problems with Shapley-value-based explanations as feature importance measures. Proc. 37th Int. Conf. Mach. Learn. 119, 5491–5500.

Liu, H.-H., Zhang, J., Liang, F., Temizel, C., Basri, M.A., Mesdour, R., 2021. Incorporation of physics into machine learning for production prediction from unconventional reservoirs: a brief review of the gray-box approach. SPE Reservoir Eval. Eng. 24 (4), 847–858. https://doi.org/10.2118/205520-PA.

Luffel, D.L., Guidry, F.K., 1992. New core analysis methods for measuring reservoir rock properties of devonian shale. J. Petrol. Technol. 44 (11), 1184–1190. https://doi.org/10.2118/20571-PA.

Morriss, C., Rossini, D., Straley, C., Tutunjian, P., Vinegar, H., 1997. Core analysis by low-field nmr. Log. Anal. 38 (2).

Okoli, C.O., Goddard, S.D., Awoleke, O.O., 2023. Uncertainty quantification in the Permian Basin using conventional and modified bootstrap methodology. Petrol. Res. 8 (4), 439–454. https://doi.org/10.1016/j.ptlrs.2023.06.001.

Patrick Murphy, D., Chilingarian, G, V., Jalal Torabzadeh, S., 1996. Chapter 3 Core analysis and its application in reservoir characterization. In: Chilingarian, G. V., Mazzullo, S.J., Rieke, H.H. (Eds.), Developments in Petroleum Science, vol. 44. Elsevier, pp. 105–153. https://doi.org/10.1016/S0376-7361(96)80025-2.

Pugh, V.J., Thomas, D.C., 1989. A statistical analysis of the accuracy and reproducibility of standard core analysis. Log. Anal. 30 (2).

Qajar, J., Arns, C.H., 2022. Chemically induced evolution of morphological and connectivity characteristics of pore space of complex carbonate rock via digital core analysis. Water Resour. Res. 58 (3), e2021WR031298. https://doi.org/10.1029/2021WR031298.

Rao, H., Shi, X., Rodrigue, A.K., Feng, J., Xia, Y., Elhoseny, M., Yuan, X., Gu, L., 2019. Feature selection based on artificial bee colony and gradient boosting decision tree. Appl. Soft Comput. 74, 634–642. https://doi.org/10.1016/j.asoc.2018.10.036.

Rothwell, R.G., Rack, F.R., 2006. New techniques in sediment core analysis: an introduction. Geol. Soc. London, Spec. Publ. 267 (1), 1–29. https://doi.org/10.1144/GSL.SP.2006.267.01.01.

Shafer, J., 2013. Recent advances in core analysis. Petrophys. - SPWLA J. 54 (6), 554–579.

Sun, R., Wang, G., Zhang, W., Hsu, L.-T., Ochieng, W.Y., 2020. A gradient boosting decision tree based GPS signal reception classification algorithm. Appl. Soft Comput. 86, 105942. https://doi.org/10.1016/j.asoc.2019.105942.

Yang, K., Connolly, P.R.J., Li, M., Seltzer, S.J., McCarty, D.K., Mahmoud, M., El-Husseiny, A., May, E.F., Johns, M.L., 2020. Shale rock core analysis using NMR: effect of bitumen and water content. J. Petrol. Sci. Eng. 195, 107847. https://doi.org/10.1016/j.petrol.2020.107847.

Yousef, I., Morozov, V.P., 2024. Exploring the potential of drill cuttings for reservoir characterization: a case study from the Volga-Ural basin, Russia. Petrol. Res. 9 (2), 193–205. https://doi.org/10.1016/j.ptlrs.2024.01.012.